Appl Phys A (2010) 98: 855–860
DOI 10.1007/s00339-010-5552-0

Applied Physics A
Materials Science & Processing

A method to fabricate 2D nanoparticle arrays

C.H. Lin · L. Jiang · Y.H. Chai · H. Xiao · S.J. Chen · H.L. Tsai

Received: 27 August 2009 / Accepted: 6 January 2010 / Published online: 27 January 2010
© Springer-Verlag 2010

Abstract This article demonstrates an efficient approach to fabricate nanoparticles arranged in a periodic pattern over a large area. A nanoscale gold film coated on a silicon wafer substrate was sectioned into grids by focused ion beam machining. Through a thermal treatment, the film in a confined area transforms into a nanoparticle due to the surface tension effect of the melted gold film. By controlling the film thickness and the size of the confined area, a nanoparticle array with various particle sizes and interparticle spacings can be manipulated. This approach may have great potential applications in sensor chips and nonlinear devices.

1 Introduction

Periodic nanostructures can significantly enhance the optical nonlinear properties [1, 2] and intensify the electromagnetic field for metal particles [3, 4]. Recently, two-dimensional (2D) periodic nanopatterning has attracted much attention because of its broad applications, including Raman-active substrates [5, 6], photonics [7, 8], data storage [9], and other applications [10, 11]. The optical properties of nanostructures are determined by factors such as the composition, crystallinity, size, shape, as well as the pattern and the interparticle spacing. Hence, a simple and effective approach to produce a large area of nanoparticle arrays with the capability to manipulate the particle size and interparticle spacing is important for ultra-sensitive sensing applications or nonlinear optical devices.

In general, nanoclusters can be well arranged in a large area by nanosphere lithography [12] to form nanoisland arrays and, then, the nanoisland arrays can be transformed into nanoparticle arrays by thermal treatment [13] or laser annealing [14]. The major limitation of this approach is that only hexagonal geometry can be obtained although the angle-resolved deposition process can slightly manipulate the arrangement [7]. To produce particle arrays in an arbitrary geometry, electron beam (E-beam) lithography (EBL) is the most popular approach to control nanostructures in arbitrary arrangement [15] but the inextricable processes including the E-beam sensitive polymer layer coating, E-beam exposing and developing, metal film coating, and lift-out process are time consuming. A simple approach, laser-induced forward transfer (LIFT) using a nanosecond laser [16] or a femtosecond laser [17], can arrange micro/nanoscale particles in an arbitrary geometry. However, in the LIFT technique, it is difficult to control the interparticle spacing in the submicron scale and to achieve a large area of particle arrays since the particles are produced one by one.

In this article, a simple and efficient approach to form an arbitrary geometry of 2D gold nanoparticle arrays was in-

C.H. Lin · S.J. Chen
Department of Engineering Science, National Cheng Kung University, Tainan 70101, Taiwan

C.H. Lin · H.L. Tsai (✉)
Department of Mechanical and Aerospace Engineering, Missouri University of Science and Technology, Rolla, MO 65409, USA
e-mail: tsai@mst.edu
Fax: +1-573-3414607

L. Jiang
Department of Mechanical and Automation Engineering, Beijing Institute of Technology, Beijing 100081, China

Y.H. Chai
Department of Electrical Engineering, Technology and Science Institute of Northern Taiwan, Taipei 112, Taiwan

H. Xiao
Department of Electrical and Computer Engineering, Missouri University of Science and Technology, Rolla, MO 65409, USA

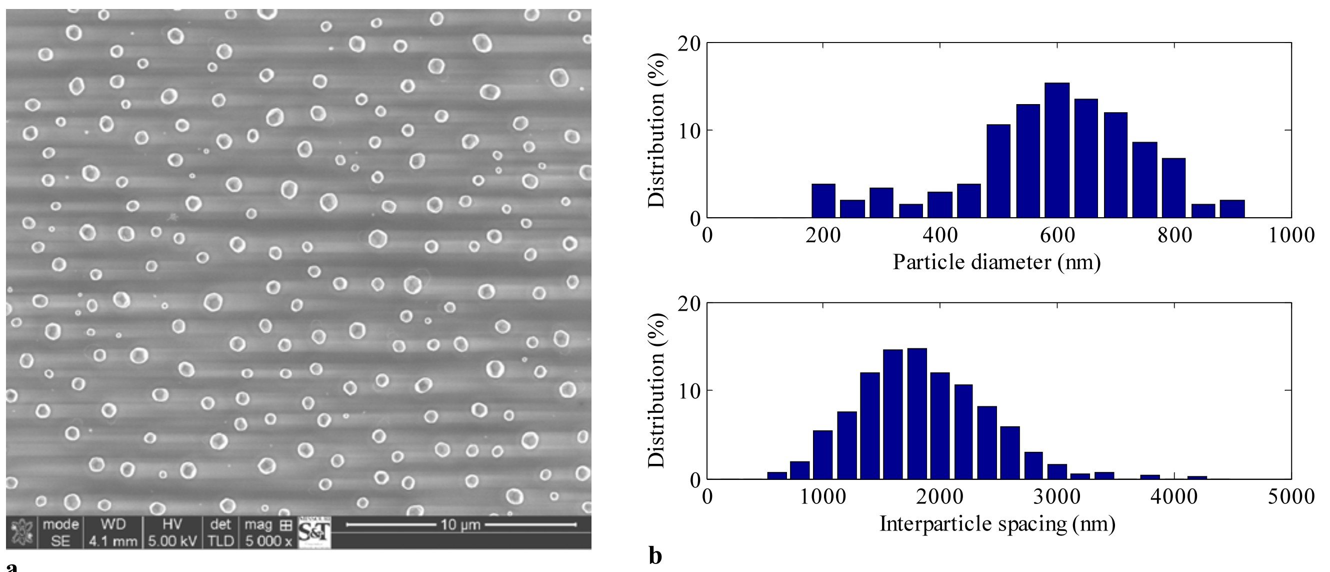

Fig. 1 Particle distribution annealed from a 20-nm bare gold thin film. **a** SEM image; **b** distributions of particle size and interparticle spacing

vestigated. This approach is a suitable platform to produce well-arranged nanoparticle arrays over a large area for different applications.

2 Experimental

In this work, polished silicon wafers were employed as substrates due to their high surface flatness and high melting temperature. Small pieces of silicon wafer were prepared and cleaned in an ultrasonic bath with methanol for 10 min and rinsed with de-ionized water for another 10 min. The rinsed substrates were baked dry on a hot plate for 5 min. Gold thin films were coated on cleaned silicon wafer substrates via a RF sputter coater with a thickness of 10 nm, 20 nm, or 30 nm. The RF power of the coater was set as 100 W, which corresponds to the deposition rate of around 20 nm/min. The ion source of the focused ion beam (FIB) (Helios NanoLab 600 FIB/FESEM, FEI) is gallium and the current density was adjusted to achieve the material removal rate of 4.125×10^6 nm^3/s. In order to engrave desired nanoscale patterns on the substrate efficiently, the dual-beam focused ion beam was operated at the 'scanning mode' rather than being manually controlled. A 24-bit color picture in BMP format with the size of 3072 pixels × 3072 pixels (x-direction × y-direction) was designed and generated by commercial image processing software. The pattern employed in this work is grid arrays with the grid period of 32 pixels × 32 pixels, and the line width between two grids is one pixel in either the x- or y-direction. The picture was loaded in the operating software of the FIB system and was scaled into squares with the overall dimensions of 18 μm × 18 μm, 24 μm × 24 μm, or 30 μm × 30 μm. This will allow us to study the effect of different pitches of grid on the particle size. The engraved depth was set as slightly deeper than the thickness of the gold film to assure that every square unit in the grid array has a clean cut without any connection between adjacent grids. After the pattern of periodic nanoscale grids with the desired size was engraved by the FIB machining process, the samples were thermally treated in a programmable furnace (Fisher Scientific). The temperature was first ramped up to 1080°C at 10°C/min that is slightly higher than the melting temperature of gold and, then, the temperature was held for 5 min. Finally, the furnace was turned off and the sample remained inside the furnace until the temperature cooled to room temperature. The fabricated nanoscale particle arrays were examined via a field-emission scanning electron microscope (FESEM) which is integrated in the FIB equipment.

3 Results and discussion

Figure 1a shows the FESEM image of particles on a wafer substrate of an annealed 20-nm-thick gold film without area confinement. It is seen that the distributions of particle size and interparticle spacing are quite random. The distributions of the particle size and interparticle spacing were analyzed and the statistics data are shown in Fig. 1b. The distributions show a broad range of particle size from 200 nm to 900 nm and an interparticle spacing from 600 nm to 4200 nm. The standard deviations of the particle size and interparticle spacing are, respectively, 155.5 nm and 553.3 nm. Note that the interparticle spacing for each particle is defined as the center-to-center distance between the particle and its four adjacent particles. For each particle theoretically there

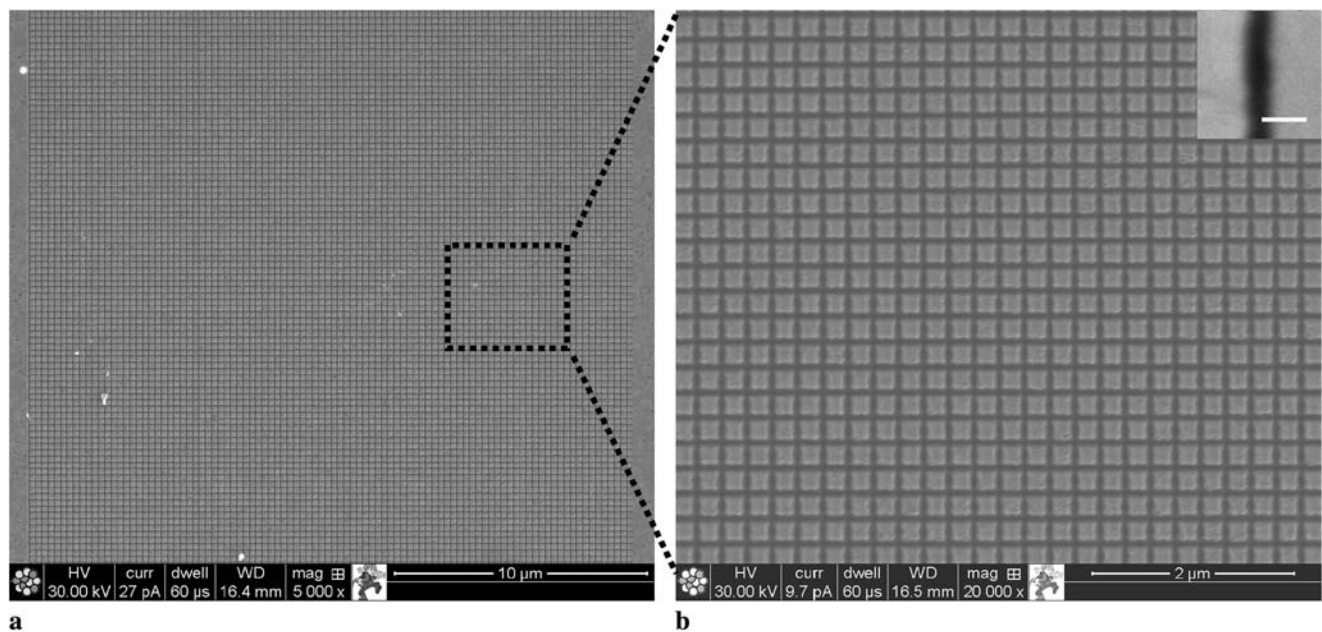

Fig. 2 SEM images of the gold thin film after patterning by FIB. **a** Large-area image; **b** enlarged image. The *scale bar* in the *inset* is 50 nm

are four interparticle segments (2D case). However, each interparticle segment cannot be double counted and, hence, the maximum number of interparticle segments is two for each particle. In the case of the annealed bare gold film, the particle size is determined by the local surface tension of the melted gold film, which, in turn, depends on the variations of local substrate conditions and the thickness of the gold film. This kind of particle array is unsuitable for applications because of the random distributions of particle size and interparticle spacing.

Figure 2a shows the FESEM image of the 2D periodic grids for a gold film with 20-nm thickness on a wafer substrate obtained by means of FIB machining. Compared to the conventional manual operation, the scanning mode takes less than 2 min to engrave the pattern of the size 24 µm $\times$ 24 µm with 20-nm depth. The enlarged image of the engraved pattern is shown in Fig. 2b. As shown in Fig. 2b, the size of the grids appears to be highly uniform and the boundaries of each square have a clean cut without connection between adjacent grids. The engraved line width between adjacent grids is 50 nm on average and is 30 nm minimum (as shown in the inset of Fig. 2b), which corresponds to one pixel of a 24-bit color picture in BMP format. The pitch of the grids is 250 nm and the size of each square unit is 200 nm $\times$ 200 nm due to the 50-nm line width. After thermal treatment, the square film array transforms to a particle array and each particle is confined in a square lattice. Figure 3a shows the image of a large region including the engraved grids and its surrounding areas. It is seen that the surrounding areas without FIB engraving have relatively large particles and random distributions of particle size and location, while, in the engraved grids, much smaller and uniform particles are found and they are well arranged, Fig. 3b. The square gold films were melted when the temperature was higher than the melting temperature, balled into round droplets by surface tension, and solidified when the temperature was cooling down. There is no apparent ‘scratch’ on the substrate as shown in Fig. 3b, which implies that the engraving process has just removed the gold film without physically over-cutting into the substrate. However, some material properties of the substrate might be affected by the high-energy ions.

Two additional experiments were conducted to study the effects of gold film thickness and grid pitch on the particle size and interparticle spacing. Figure 4 shows the distributions of particle diameter for a film thickness of 10 nm (case 1), 20 nm (case 2), and 30 nm (case 3) with a grid pitch of 250 nm; their average diameters are, respectively, 103.6 nm, 132.1 nm, and 153.1 nm, Fig. 4a. The corresponding standard deviations are 4.7 nm, 2.7 nm, and 2.6 nm. The interparticle spacing is defined in the same way as before, except that all particles are about the same size in each case of film thickness. The distributions of interparticle spacing are given in Fig. 4b, and the averages of the interparticle spacing are, respectively, 247.6 nm, 249.5 nm, and 250.8 nm. The standard deviations of the interparticle spacing are, respectively, 20.8 nm, 19.0 nm, and 15.9 nm. The experimental results reveal, for the same grid size, that a thicker film can achieve more uniform (smaller standard deviation) particle size and interparticle spacing. In fact, from the deposition standpoint, it is not easy to perform coating of a 10-nm-thick film with high

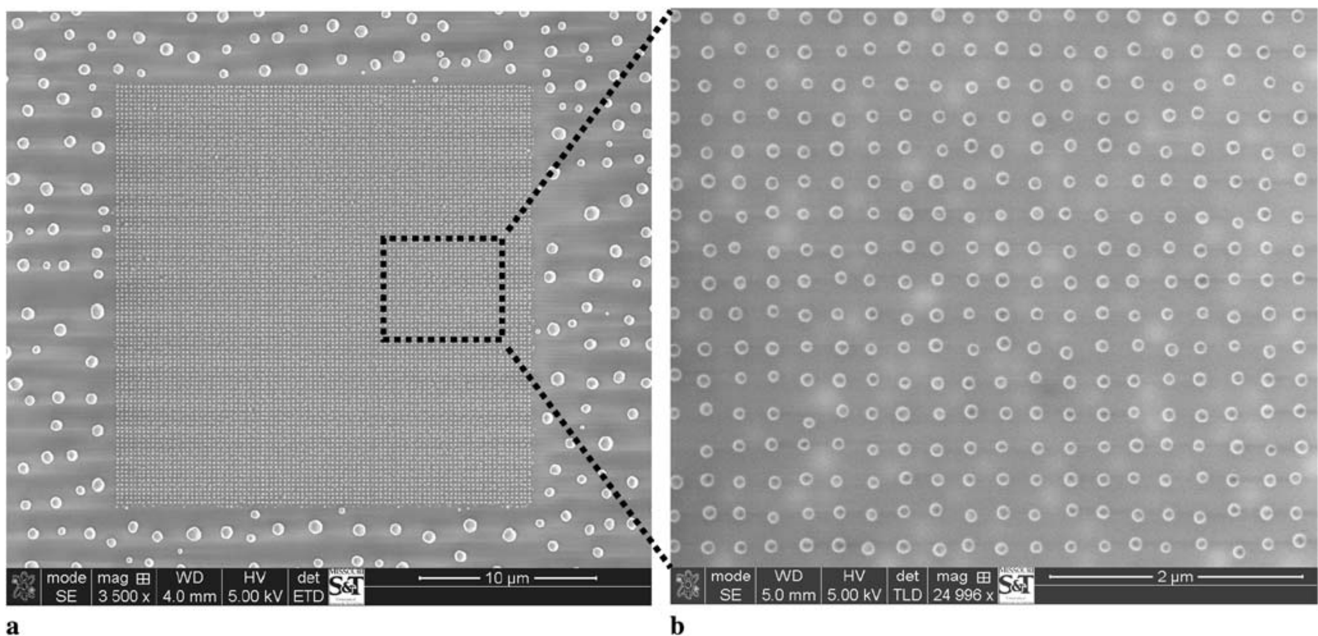

Fig. 3 SEM images of the fabricated particle array. **a** Overview of the particle array in a 24 μm × 24 μm patterned area; **b** enlarged image of the engraved region

uniformity. Hence, it is expected to have some thickness variation across the entire substrate for a 10-nm-thick film (case 1), which may lead to a greater standard deviation of the particle size. In this experiment, the area of each square grid is identical for all three cases, so the variation of thickness becomes an important factor that causes the variation of particle diameter. However, as the film thickness increases, the effect of thickness variation on particle size decreases. For example, assuming that there is a 1-nm thickness variation on the substrate for a RF sputter coater, this 1-nm thickness variation causes a much greater 'deviation' for a 10-nm coating than for a 30-nm coating.

Different pitches of grids, 187.5 nm × 187.5 nm (size 1), 250 nm × 250 nm (size 2), and 312.5 nm × 312.5 nm (size 3), were patterned on a gold film with 10-nm thickness. Figure 5a shows that the distributions of particle diameter and the average diameters for size 1, size 2, and size 3 are, respectively, 75.4 nm, 110.8 nm, and 142.9 nm. The corresponding standard deviations are, respectively, 4.6 nm, 4.4 nm, and 4.3 nm. Figure 5b shows that the distributions of interparticle spacing and the averages are 185.6 nm, 249.9 nm, and 310.5 nm for size 1, size 2, and size 3, which agree with the designed grid size. The corresponding standard deviations are 7.1 nm, 21.7 nm, and 45.0 nm. The results show that, for the same film thickness, as the square area increases, the uniformity of the particle diameter increases, but the uniformity of the interparticle spacing decreases. Note that, when the pitch of the grid exceeds some critical value, it is possible that more than one particle can be present in a grid and their locations can be randomly distributed, similar to the case as discussed in Fig. 1 when there is no area confinement.

The temperature of the thermal treatment is important and directly affects the formation of particles. For small-sized particles, lower temperatures below the melting temperature of gold (950°C) are able to induce surface melting around the particle with a thickness of a few nanometers [18]. When the treating temperature is lower than the melting temperature, the square gold film starts to melt from its outer edges, particularly the four corners. This is because, at the edges/corners, the film has a higher surface-to-volume ratio which can be more efficiently heated up. Once the treating temperature is ramped up to a temperature higher than the melting temperature, the solid square film becomes a round-edged shape and the melting is toward the center of the square. Finally, the melted square film balls into a spherical particle caused by the surface tension effect. It is assumed that the patterned film consists of perfect squares and the condition at the interface between the gold film and the substrate is identical. Under these assumptions, the surface tension provides an identical driving force to gradually pull the melted portion of the gold film, starting from the edges of the square, toward the center of the square, which results in the interparticle spacing with small standard deviation as discussed above.

In this work, the square lattice nanoparticle arrays were demonstrated. This technology can be extended to produce nanoparticle patterns arranged in desired geometries, including a combination of different particle sizes. Furthermore,

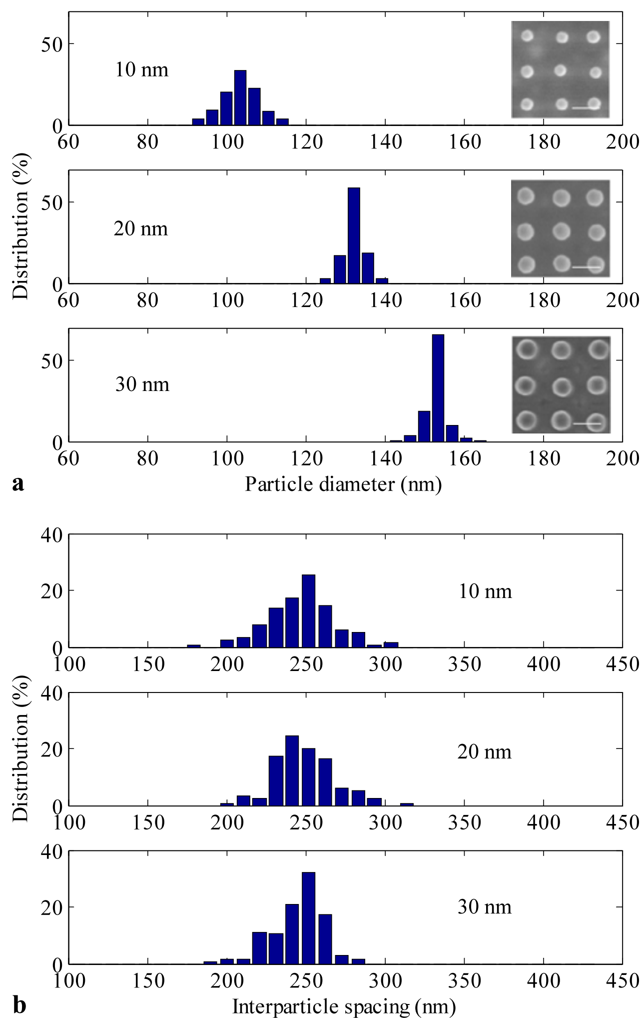

Fig. 4 Statistics of nanoparticle arrays fabricated from 250-nm-pitch grids patterned on gold films of 10-nm, 20-nm, or 30-nm thickness. **a** Particle diameter. The *scale bar* in the *inset* is 200 nm; **b** interparticle spacing

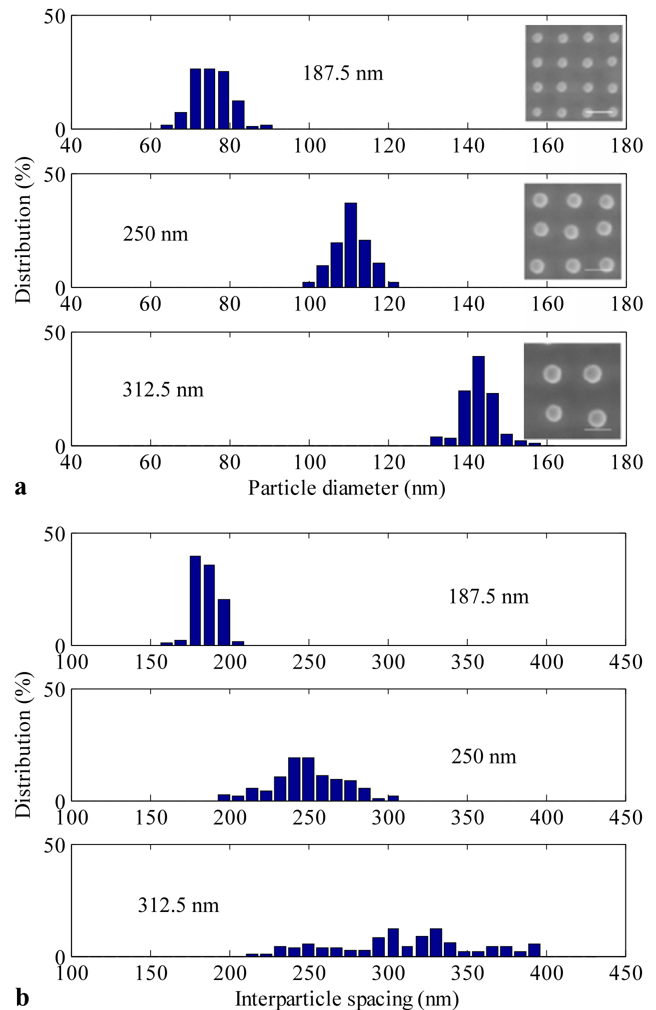

Fig. 5 Statistics of nanoparticle arrays fabricated from 10-nm gold films patterned on grids with different pitches of 187.5 nm, 250 nm, or 312.5 nm. **a** Particle diameter. The *scale bar* in the *inset* is 200 nm; **b** interparticle spacing

different materials can be coated on the same substrate to achieve desirable functionalities of the nanoparticle array.

4 Conclusions

By using a FIB to confine the thin-film area, followed by a thermal annealing process, gold nanoparticle arrays were fabricated. The particle size and interparticle spacing can be manipulated by controlling the thickness of the thin film and the size of the confined area. The proposed method is simple and rapid as compared to other approaches and provides another way of fabricating functional devices, such as a surface enhanced Raman scattering sensor which is sensitive to different metals, particle size, and interparticle spacing.

Acknowledgement This work was partially supported by the US Department of Energy under Contract No. DE-FE0001127 and the National Natural Science Foundation of China under Grant No. 90923039.

References

1. W. Wang, Y. Wang, Z. Dai, Y. Sun, Y. Sun, Appl. Surf. Sci. **253**, 4673 (2007)
2. H. Shen, B. Cheng, G. Lu, T. Ning, D. Guan, Y. Zhou, Z. Chen, Nanotechnology **17**, 4274 (2006)
3. N. Nedyalkov, T. Sakai, T. Miyanishi, M. Obara, Appl. Phys. Lett. **90**, 123106 (2007)
4. D.A. Genov, A.K. Sarychev, V.M. Shalaev, A. Wei, Nano Lett. **4**, 153 (2004)
5. C. Fang, A. Agarwal, K.D. Buddharaju, N.M. Khalid, S.M. Salim, E. Widjaja, M.V. Garland, Biosens. Bioelectron. **24**, 216 (2008)
6. G. Duan, W. Cai, Y. Luo, Y. Li, Y. Lei, Appl. Phys. Lett. **89**, 181918 (2006)
7. C.L. Haynes, R.P. Van Duyne, Nano Lett. **3**, 939 (2003)
8. C.L. Haynes, A.D. McFarland, L. Zhao, R.P. Van Duyne, G.C. Schatz, L. Gunnarsson, J. Prikulis, B. Kasemo, M. Kill, J. Phys. Chem. B **107**, 7337 (2003)
9. J. Sort, H. Glaczyuska, U. Ebels, B. Dieny, M. Giersig, J. Rybczynski, J. Appl. Phys. **95**, 7516 (2004)
10. S. Enoch, R. Quidant, G. Badenes, Opt. Express **12**, 3422 (2004)

11. S.H. Lim, W. Mar, P. Matheu, D. Derkacs, E.T. Yu, J. Appl. Phys. **101**, 104309 (2007)
12. M. Winzer, M. Kleiber, N. Dix, R. Wiesendanger, Appl. Phys. A **63**, 617 (1996)
13. H.A. Bullen, S.J. Garrett, Nano Lett. **2**, 739 (2002)
14. F. Sun, W. Cai, Y. Li, G. Duan, W.T. Nichols, C. Liang, N. Koshizaki, Q. Fang, I.W. Boyd, Appl. Phys. B **81**, 765 (2005)
15. D.R.S. Cumming, S. Thoms, S.P. Beaumont, J.M.R. Weaver, Appl. Phys. Lett. **68**, 15 (1996)
16. D.A. Willis, V. Grosu, Appl. Phys. Lett. **86**, 244103 (2005)
17. D.P. Banks, C. Grivas, J.D. Mills, R.W. Eason, L. Zergioti, Appl. Phys. Lett. **89**, 193107 (2006)
18. S. Inasawa, M. Sugiyama, Y. Yamaguchi, J. Phys. Chem. B **109**, 3104 (2005)